Graphene–Biomineral Hybrid Materials

*Sungjin Kim, Sook Hee Ku, Seong Yoon Lim, Jae Hong Kim, and Chan Beum Park**

Graphene, an sp^2-bonded carbon sheet with a thickness of single atom, has recently received attention from materials scientists because of its unique qualities, which include excellent thermal and mechanical properties and electrical conductivity resulting from long-range π-conjugation.[1–5] While graphene was originally developed for nanoelectronics applications,[1,6,7] research interests in graphene are continuously expanding to other fields.[1,2] For example, graphene is considered to be an adequate reinforcing component for composite materials.[3,5,8,9] However, hybridization or interaction of graphene with biominerals has so far been rarely reported. Biomineralization is the process that gives rise to small and large inorganic-based structures in biological systems, and it often results in sophisticated materials having elaborate morphologies, excellent mechanical and optical properties, and vital biological functions.[10–13] Thus, the convergence of the study of graphene with biomineralization is expected to widen the horizons of material science.

We have successfully incorporated graphene and graphene oxide (GO) sheets into the crystals of the two most abundantly studied biominerals found in the hard tissues of invertebrates and vertebrtates: calcium carbonate[14–16] and calcium phosphate.[17,18] As illustrated in **Scheme 1**, we used GO sheets for the synthesis of a graphene–$CaCO_3$ hybrid film, which then underwent a transformation into graphene-incorporated hydroxyapaptite [$Ca_{10}(PO_4)_6(OH)_2$; HAp]. By applying CO_2 gas to a mixture of GO and $CaCl_2$, we obtained spherical $CaCO_3$ vaterite microspheres that were wrapped and interconnected by a GO network. After the reduction of GO–$CaCO_3$ composite, we fabricated a conductive, biocompatible, and bone-bioactive hybrid film that consisted of $CaCO_3$ microspheres interconnected with a graphene network. When incubated in simulated body fluid (SBF), the graphene–$CaCO_3$ hybrid film was transformed to graphene-incorporated bone HAp crystals. We further found that osteoblast cells adhered well and proliferated on the graphene–HAp composite.

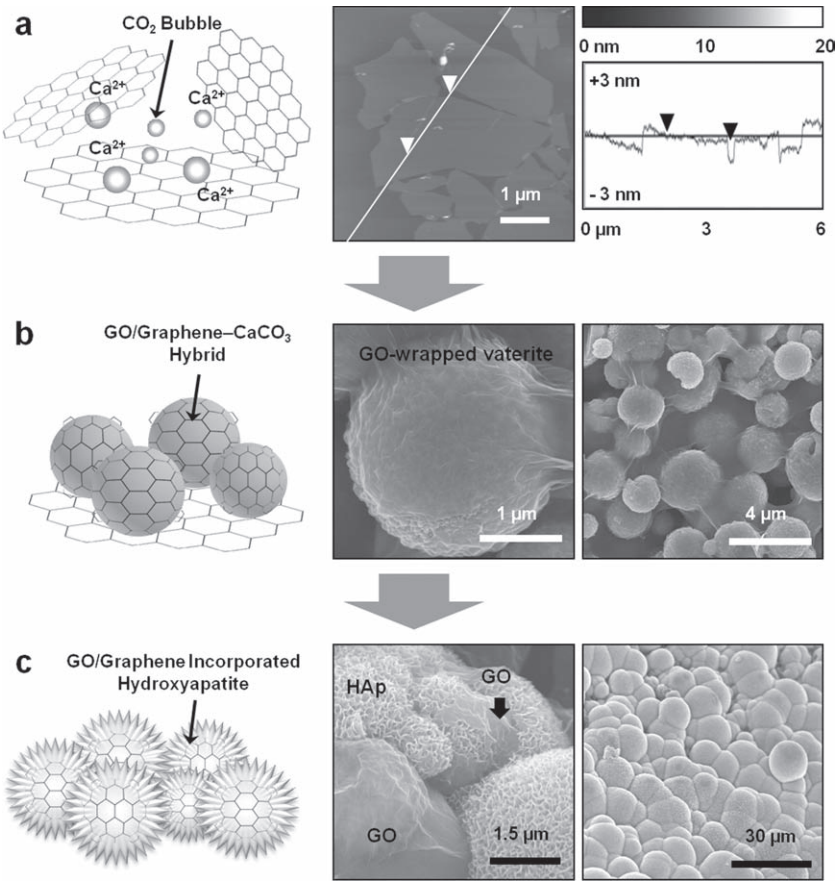

Scheme 1. Illustration of GO/graphene–$CaCO_3$ hybrid material synthesis and its conversion to GO/graphene–hydroxyapatite (HAp) composites. The steps describe a) CO_2 mineralization to $CaCO_3$ in the presence of GO sheets and $CaCl_2$, b) GO/graphene–$CaCO_3$ hybrid materials, and c) their conversion to GO/graphene–HAp hybrid materials. Images in the right column show a) an AFM image and sectional analysis of graphene oxide (GO) sheets used for this study, b) SEM images of GO-wrapped vaterite microspheres, and c) SEM images of GO–HAp hybrid film that show HAp surrounding GO sheets and covering the entire film surface.

We prepared GO sheets from pristine graphite according to the modified Hummers method.[19–21] Atomic force microscopy (AFM) analysis showed that single-layered GO sheets approximately 1.06 nm thick were successfully attained from pristine graphite (Scheme 1), which is in agreement with previous reports.[21–23] The characteristics of GO sheets were further confirmed using X-ray diffraction (XRD) measurements (Figure S1, Supporting Information). After introducing CO_2 gas into a solution containing exfoliated GO and $CaCl_2$, followed by filtering and drying the resultant suspension, we synthesized a rigid,

S. Kim, S. H. Ku, S. Y. Lim, J. H. Kim, Prof. C. B. Park
Department of Materials Science and Engineering
Korea Advanced Institute of Science and Technology (KAIST)
335 Science Road, Daejeon 305-701, Republic of Korea
E-mail: parkcb@kaist.ac.kr

DOI: 10.1002/adma.201100010

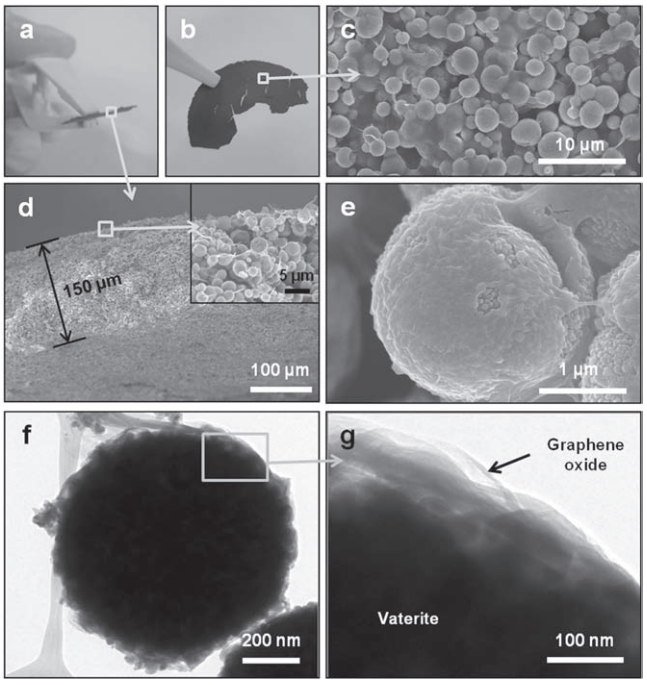

Figure 1. Digital camera images of synthesized GO–$CaCO_3$ hybrid film showing its a) side view and b) front view. c) SEM image of a GO–$CaCO_3$ hybrid film surface composed of vaterite microspheres hybridized with GO sheets. d) SEM image of GO–$CaCO_3$ hybrid film (side view) showing vaterite microspheres stacked up to the thickness of 150 μm. e) An individual GO–$CaCO_3$ microsphere showing the morphology of a GO sheet stretched to wrap a vaterite microsphere. TEM images of f) an individual GO–$CaCO_3$ microsphere and g) a magnified image showing a GO sheet covering the surface of a vaterite microsphere.

self-standing GO–$CaCO_3$ hybrid film that consisted of numerous $CaCO_3$ microspheres interconnected by a GO network (**Figure 1**). The thickness of the hybrid film was approximately 150 μm (Figure 1d) and could be controlled by adjusting the amount of suspension during the filteration process. Each microsphere was apparently "wrapped" by well-stretched GO sheets, as shown in the scanning electron microscopy (SEM) image (Figure 1e) and transmission electron microscopy (TEM) images (Figure 1f,g). Transparent GO sheets were also found inside broken microspheres (Figure S2a, Supporting Information) and interconnected between the microspheres (Figure S2b).

The attained GO–$CaCO_3$ hybrid film was further reduced by treating it with hydrazine. Raman spectra of hybrid films before and after the reduction (**Figure 2**a) showed peaks of the D band (disorder band caused by the graphite edges) and G band (in-phase vibration band of graphite lattice) at 1345 and 1590 cm^{-1}, respectively,[24] while no peaks were found at the two wavelengths in the Raman spectrum corresponding to pure $CaCO_3$. A slightly increased D/G intensity ratio of GO was observed after the reduction, which according to previous reports indicates the successful conversion of GO into graphene.[21,25,26] According to the cyclic voltammetric analysis (Figure S3, Supporting Information), the reduced GO-$CaCO_3$ (i.e., graphene–$CaCO_3$) hybrid film exhibited highly increased electrical capacitance, which implies that the GO network was well converted into an electrically conductive graphene

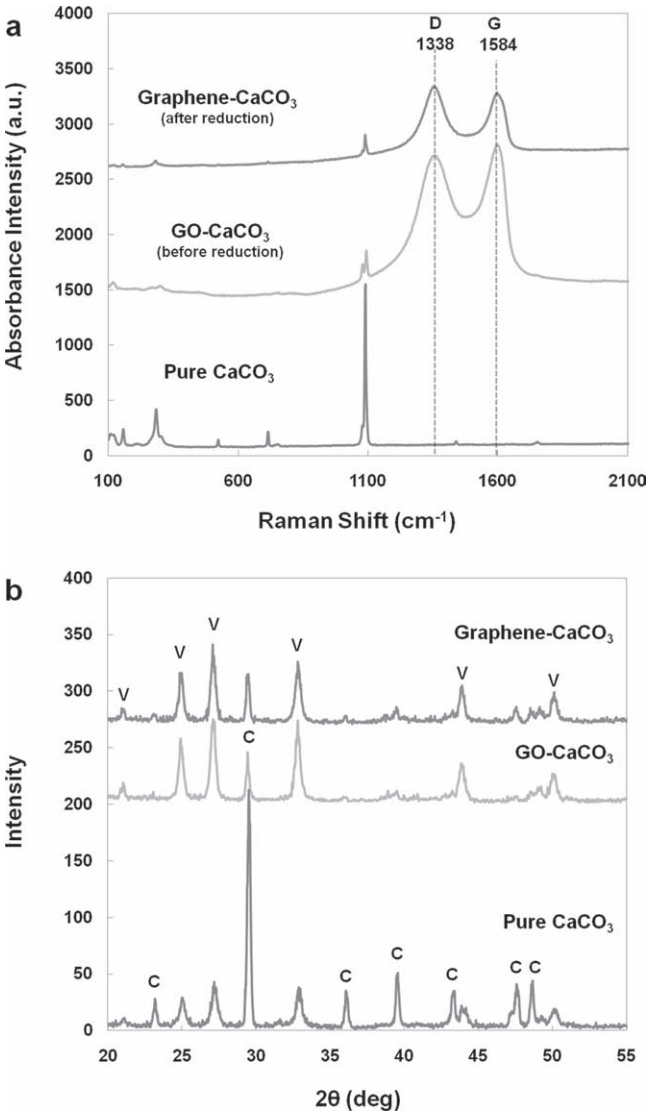

Figure 2. Raman spectra and XRD patterns of pure $CaCO_3$ (mineralized without GO) and $CaCO_3$ mineralized with GO before and after the reduction of GO-$CaCO_3$. a) Raman spectra of $CaCO_3$ mineralized in the presence of GO shows two bands at 1338 and 1584 cm^{-1}, the D and G bands, respectively. The D/G intensity ratio increased after reduction with hydrazine. b) The XRD analysis shows that the ratio of peak intensity for vaterite to calcite significantly increased when GO was present in the mineralization. The ratio was maintained even after the chemical reduction of GO–$CaCO_3$. C and V indicate calcite and vaterite, respectively.

network. XRD measurements (Figure 2b) show that the ratio of vaterite (PDF card #33-0268) to calcite (PDF card #47-1743) is much higher in the GO– and graphene–$CaCO_3$ hybrid films than in the pure $CaCO_3$, indicating that most $CaCO_3$ microspheres found in the hybrid films are vaterite crystals, the most unstable crystalline polymorph of $CaCO_3$. In contrast, rhombohedral calcite crystals were dominantly found for $CaCO_3$ mineralized in the absence of GO sheets (Figure S4, Supporting Information). It is known that the vaterite, a hexagonal crystal that typically grows in a spherical form, rapidly transforms to the stable calcite phase with rhombohedral crystalline structure

that does not undergo any further phase transition in aqueous solution.[10] The overall structure of $CaCO_3$ vaterite microspheres, which were wrapped by a GO or graphene network, was well preserved after the reduction process (Figure S5, Supporting Information). Note that the graphene–$CaCO_3$ hybrid film could not be synthesized directly using graphene and CO_2 gas because of severe aggregation of graphene sheets during biomineralization.

The formation of $CaCO_3$ vaterite microspheres in the presence of GO sheets is attributed to the residing functional groups of GO sheets, such as hydroxyl, epoxy, carboxylic acid, and other carbonyl groups,[27–29] that can favorably interact with Ca^{2+} in vaterite and further prevent the dissolution of vaterite and its recrystallization to calcite. In particular, carboxylic moieties and hydroxyl groups of GO sheets should induce the formation of the vaterite phase, as their ionization results in a negatively charged surface[30] that can associate with Ca^{2+} by electrostatic interaction, which should further hinder the dissolution–recrystallization process of vaterite to calcite.[16] Furthermore, the strong mechanical strength of the GO network surrounding $CaCO_3$ microspheres may also contribute to slowing their crystal growth and morphological transformation into rhombohedral calcite (Figure S4, Supporting Information). This suggestion is supported by a previous study,[31] which reported that carboxyl-functionalized carbon nanotubes (CNT–COOH) can stabilize the vaterite phase through the electrostatic interaction between carboxyl groups of CNT–COOH and the mechanically strong framework surrounding the spherical vaterite microstructure.

To assess the in vitro bone bioactivity of GO–$CaCO_3$ and graphene–$CaCO_3$ hybrid films, we incubated them in a SBF solution. For comparison, we also tested films of stacked, bare GO and graphene sheets, which were prepared according to Dikin et al.[32] and Li et al.,[30] respectively. The osteoconductivity of a material is widely assessed in vitro by measuring the rate of apatite formation in a SBF solution.[33–35] We found that lath-like bone HAp crystals formed in both hybrid films (**Figure 3**A-b,B-b) after 4 d of incubation, in contrast to bare GO and graphene

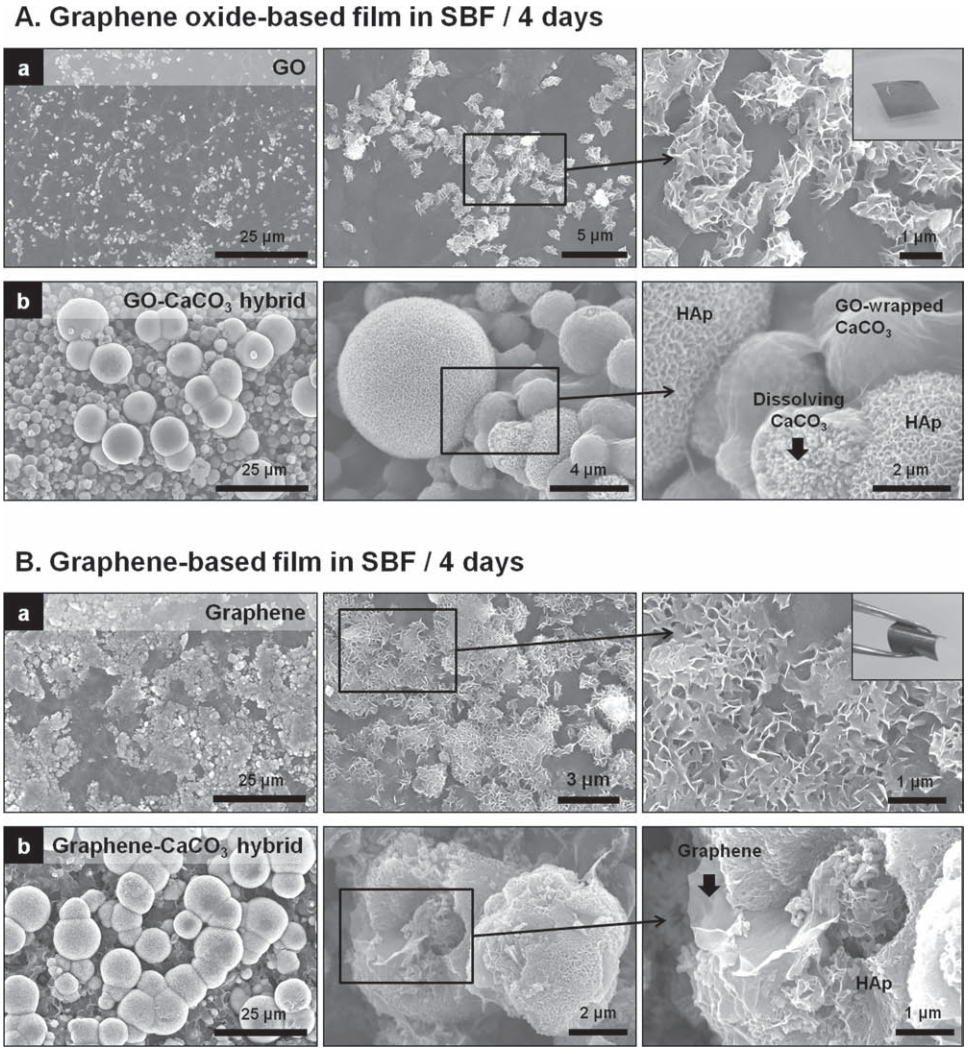

Figure 3. A) SEM images of a) bare GO film and b) GO–$CaCO_3$ hybrid film incubated in SBF for 4 d. B) SEM images of a) bare graphene film and b) graphene–$CaCO_3$ hybrid film incubated in SBF for 4 d. Both hybrid films hybridized with vaterite (A-b, B-b) showed highly increased formation of lath-like HAp crystals compared to bare GO (A-a) and bare graphene (B-a) films.

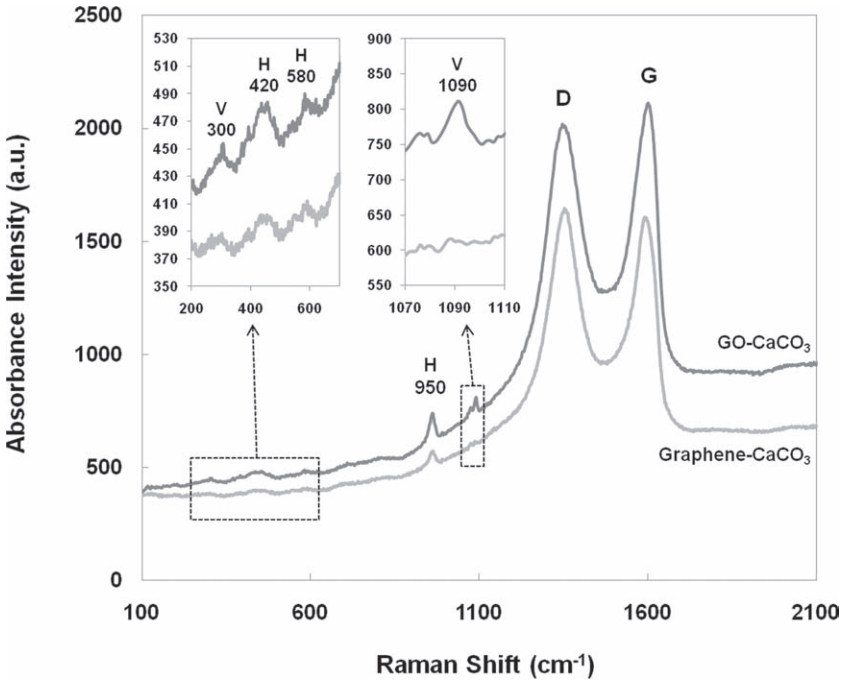

Figure 4. Raman spectra of GO/graphene–$CaCO_3$ hybrid films incubated in SBF for 4 d. Both spectra show characteristic bands at around 420, 580, and 950 cm^{-1}, indicating HAp formation. The peak intensities for $CaCO_3$ vaterite at around 300 and 1090 cm^{-1} decreased in the graphene–$CaCO_3$ hybrid film.

films, which exhibited much less apatite formation on their surfaces (Figure 3A-a,B-a). While GO-wrapped vaterites and newly formed HAp crystals were coexistent in the GO–$CaCO_3$ hybrid film, only HAp crystals were found in the graphene–$CaCO_3$ hybrid film, indicating a major dissolution of vaterite and its reprecipitation to HAp occurred in the graphene–$CaCO_3$ hybrid film. Using Raman spectroscopy analysis (**Figure 4**), we validated the coexistence of $CaCO_3$ and HAp in the GO–$CaCO_3$ hybrid film, as its spectrum showed characteristic peaks for HAp at 420 cm^{-1} (P–O vibration), 580 cm^{-1} (O–P–O vibration), and 950 cm^{-1} (P–O stretching),[36–38] together with characteristic peaks for $CaCO_3$ at around 300 and 1090 cm^{-1}, which correspond to the Raman spectrum shown in Figure 2a. In contrast, only $CaCO_3$ peaks significantly diminished in the Raman spectrum of the graphene–$CaCO_3$ hybrid film while HAp peaks were still eminent. As discussed, slower formation of HAp in the GO–$CaCO_3$ film compared to the graphene–$CaCO_3$ film is attributed to the delayed dissolution of vaterite by the interaction of vaterite with GO. Vaterite dissolution (i.e., $CaCO_3 \rightarrow Ca^{2+} + CO_3^{2-}$) is known to accelerate the local supersaturation of Ca^{2+} to stimulate its reprecipitation to HAp where CO_3^{2-} is replaced by PO_4^{3-} in SBF.[35,38]

SEM observations of all four types of films, i.e., bare GO, bare graphene, GO–$CaCO_3$, and graphene–$CaCO_3$, incubated for a shorter time (2 d) in a SBF solution further revealed that graphene–$CaCO_3$ hybrid film highly accelerated the formation of HAp crystals (Figures S7b,c, Supporting Information) compared with other films where HAp was scarcely found (Supporting Information Figure S6a for bare GO, Figure S7a for bare graphene, and Figure S6b,c for GO–$CaCO_3$). We observed HAps that swallow graphene-wrapped $CaCO_3$ microspheres in the graphene–$CaCO_3$ hybrid film (Figure S7c, Supporting Information (upper row)) and graphene sheets incorporated in HAp crystal (Figure S7c, Supporting Information (bottom row)). The energy-dispersive X-ray spectroscopy (EDS) analysis supports these observations; lath-like crystals formed over the graphene–$CaCO_3$ hybrid film showed peaks for Ca, O, and P (Figure S8d, Supporting Information), indicating that they contain every essential element of HAp, whereas P was absent in all other films (Figures S8a–c, Supporting Information). Longer incubation of hybrid films (9 d) in a SBF solution resulted in an excessive formation of HAp crystals in both hybrid films with no $CaCO_3$ microspheres remaining (Figure S9, Supporting Information). This was further verified by the Raman spectra of both films that show no peaks for $CaCO_3$ vaterite (Figure S10, Supporting Information), indicating that all the vaterite microspheres were completely dissolved and reprecipitated to HAp.

To investigate the biocompatibility of the hybrid materials prepared in this study, we observed the viability and morphology of mouse osteoblast (MC3T3-E1) after 2 d of cultivation on the following four types of films: bare GO, bare graphene, GO–HAp, and graphene–HAp. Osteoblast produces organic components of bone matrix and assists in the deposition of calcium salts in bone tissue; thus, the study of the interaction between osteoblast cells and supporting materials is needed before in vivo applications. According to the results, most adherent cells (over 95%) were alive on all types of films, and the number of live cells was approximately 140–190 per 10^6 μm^2 area with no significant difference between samples (**Figure 5**a,b). However, cell morphology was highly affected by the film type; while cells spread well and displayed polygonal morphology on bare GO film, narrow and elongated morphology was observed on GO–HAp film. On the GO–HAp film, cells wrapped HAp (and some vaterite) microspheres and interacted with them through filamentous extensions (Figure S11, Supporting Information). The difference in cell morphology on bare graphene and graphene–HAp films was negligible compared to that on bare GO and GO–HAp films, respectively. To quantify the difference in cell morphology, we analyzed the projected cell area and the cell shape index (CSI). Note that CSI reflects the circularity of a cell with a value ranging between 0 (linear) and 1 (circular). On bare GO or graphene films, the projected cell area was around 1600–2000 μm^2. After the hybridization with HAp, the area remarkably decreased to ≈1000 μm^2 (Figure 5c). CSI was estimated to be approximately 0.64 when cells were cultured on bare GO or graphene films. The value was significantly decreased to 0.35 on HAp hybrid films, which indicates more elongated cell morphology (Figure 5d). These results indicate that cell morphology was highly affected by the hybridization of GO/graphene and biominerals. According to

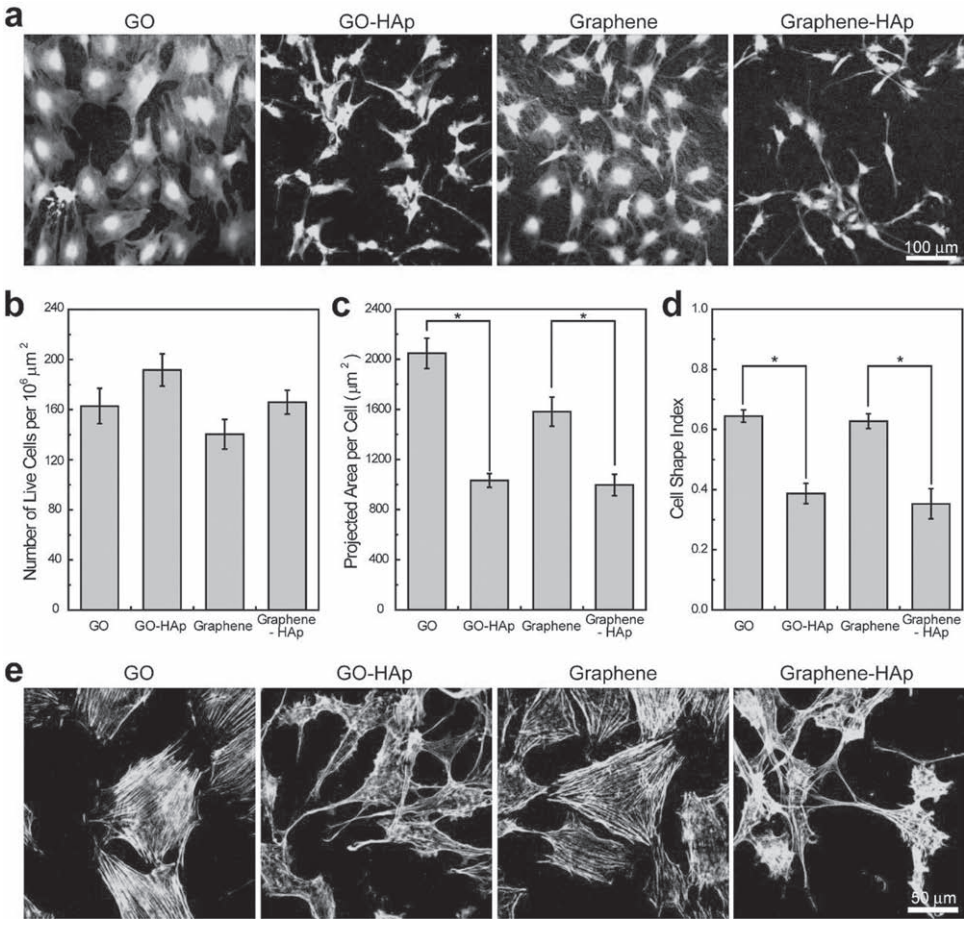

Figure 5. a) Live/dead cell assay results in the MC3T3-E1 cell culture after 2 d on GO, GO–HAp, graphene, and graphene–HAp films. b) The number of live cells per 10^6 mm^2, c) projected cell area, and d) cell shape index (CSI) were analyzed from the fluorescent images. Results are presented as mean ± standard error of the mean, and * indicates a significant difference ($p < 0.01$, one-way analysis of variance). e) Cytoskeleton organization of MC3T3-E1 cells grown on each film.

the literature,[39,40] osteoblastic cells are influenced by surface roughness and tend to elongate on rough surfaces; thus, the HAp (or vaterite) microspheres, rather than the GO/graphene with nanometer-scale thickness, may induce the adherent cells to have a more narrow morphology. We observed that the cytoskeleton of MC3T3-E1 cells were well organized with abundant stress fibers, which are the contractile bundles of actin filaments, on bare GO or graphene films, but fewer stress fibers formed when the cells were grown on hybrid HAp films (Figure 5e). The formation of stress fibers is known to be associated with focal adhesion, which is the cell–matrix junction formed by integrin when cells are grown on rigid 2D surfaces. But cell adhesion in a 3D matrix (or 3D matrix adhesion) is more biologically relevant to in vivo conditions, differs from that on 2D surface with less stress fiber formation.[41–43] The results suggest that GO/graphene–HAp hybrid materials induce a 3D matrix adhesion of osteoblast cells with high cell viability and provide a similar microenvironment to that found in vivo.

In summary, we have demonstrated the synthesis of graphene-based biomineral hybrid materials that have high in vitro bone bioactivity. The self-standing GO/graphene–$CaCO_3$ hybrid films were composed of vaterite microspheres, the most unstable crystalline polymorph of $CaCO_3$, that were wrapped and interconnected by GO (or graphene) networks. GO induced the formation of spherical vaterite crystals that maintained their shape even after the reduction of GO–$CaCO_3$ to graphene–$CaCO_3$, while rhombohedral calcite crystals were dominantly formed in the absence of GO sheets. Compared to bare GO and graphene films, GO/graphene–$CaCO_3$ hybrid materials exhibited remarkably enhanced hydroxyapatite formation when incubated in a SBF solution. The thus-formed GO/graphene–HAp composites supported high viability of osteoblast cells with elongated morphology. In vitro bone bioactivities and biocompatibility of graphene–biomineral hybrid films present the new prospect of utilizing graphene-based materials in clinical and biomedical applications.

Acknowledgements

This study was supported by the National Research Foundation (NRF) via the National Research Laboratory (R0A-2008-000-20041-0),

Engineering Research Center (2008-0062205), Converging Research Center (2009-0082276). This research was also partially supported by the Fundamental R&D Program for Core Technology of Materials from the Ministry of Knowledge Economy, Republic of Korea.

Received: January 3, 2011
Revised: February 10, 2011
Published online: March 17, 2011

[1] A. K. Geim, K. S. Novoselov, *Nat. Mater.* **2007**, *6*, 183.
[2] A. K. Geim, *Science* **2009**, *324*, 1530.
[3] S. Stankovich, D. A. Dikin, G. H. B. Dommett, K. M. Kohlhaas, E. J. Zimney, E. A. Stach, R. D. Piner, S. T. Nguyen, R. S. Ruoff, *Nature* **2006**, *442*, 282.
[4] D. Li, R. B. Kaner, *Science* **2008**, *320*, 1170.
[5] M. J. Allen, V. C. Tung, R. B. Kaner, *Chem. Rev.* **2010**, *110*, 132.
[6] K. S. Novoselov, A. K. Geim, S. V. Morozov, D. Jiang, Y. Zhang, S. V. Dubonos, I. V. Grigorieva, A. A. Firsov, *Science* **2004**, *306*, 666.
[7] Y. Kopelevich, P. Esquinazi, *Adv. Mater.* **2007**, *19*, 4559.
[8] S. Gilje, S. Han, M. Wang, K. L. Wang, R. B. Kaner, *Nano Lett.* **2007**, *7*, 3394.
[9] Y. Si, E. T. Samulski, *Nano Lett.* **2008**, *8*, 1679.
[10] S. Mann, *Biomineralization: Principles and Concepts in Bioinorganic Materials Chemistry*, Oxford University Press, Oxford, UK **2001**.
[11] L. Addadi, S. Weiner, *Angew. Chem. Int. Ed.* **1992**, *31*, 153.
[12] B. L. Smith, T. E. Schäffer, M. Viani, J. B. Thompson, N. A. Frederick, J. Kindt, A. Belcher, G. D. Stucky, D. E. Morse, P. K. Hansma, *Nature* **1999**, *399*, 761.
[13] J. Aizenberg, J. C. Weaver, M. S. Thanawala, V. C. Sundar, D. E. Morse, P. Fratzl, *Science* **2005**, *309*, 275.
[14] Y. Politi, T. Arad, E. Klein, S. Weiner, L. Addadi, *Science* **2004**, *306*, 1161.
[15] E. M. Pouget, P. H. H. Bomans, J. A. C. M. Goos, P. M. Frederik, G. de With, N. A. J. M. Sommerdjik, *Science* **2009**, *323*, 1455.
[16] S. Kim, C. B. Park, *Langmuir* **2010**, *26*, 14730.
[17] S. V. Dorozhkin, M. Epple, *Angew. Chem. Int. Ed.* **2002**, *41*, 3130.
[18] T. A. Taton, *Nature* **2001**, *412*, 491.
[19] W. S. Hummers, R. E. Offeman, *J. Am. Chem. Soc.* **1958**, *80*, 1339.
[20] N. I. Kovtyukhova, P. J. Ollivier, B. R. Martin, T. E. Mallouk, S. A. Chizhik, E. V. Buzaneva, A. D. Gorchinskiy, *Chem. Mater.* **1999**, *11*, 771.
[21] Y. Xu, H. Bai, G. Lu, C. Li, G. Shi, *J. Am. Chem. Soc.* **2008**, *130*, 5856.
[22] S. Niyogi, E. Bekyarova, M. E. Itkis, J. L. McWilliams, M. A. Hamon, R. C. Haddon, *J. Am. Chem. Soc.* **2006**, *128*, 7720.
[23] X. Li, G. Zhang, X. Bai, X. Sun, X. Wang, E. Wang, H. Dai, *Nat. Nanotechnol.* **2008**, *3*, 538.
[24] K. N. Kudin, B. Ozbas, H. C. Schniepp, R. K. Prud'homme, I. A. Aksay, R. Car, *Nano Lett.* **2008**, *8*, 36.
[25] S. Stankovich, D. A. Dikin, R. D. Piner, K. A. Kohlhaas, A. Kleinhammes, Y. Jia, Y. Wu, S. T. Nguyen, R. S. Ruoff, *Carbon* **2007**, *45*, 1558.
[26] S. Park, J. An, R. D. Piner, I. Jung, D. Yang, A. Velamakanni, S. T. Nguyen, R. S. Ruoff, *Chem. Mater.* **2008**, *20*, 6592.
[27] W. Gao, L. B. Alemany, L. Ci, P. M. Ajayan, *Nat. Chem.* **2009**, *1*, 403.
[28] F. Liu, T. S. Seo, *Adv. Funct. Mater.* **2010**, *20*, 1930.
[29] S. Park, R. S. Ruoff, *Nat. Nanotechnol.* **2009**, *4*, 217.
[30] D. Li, M. B. Müller, S. Gilje, R. B. Kaner, G. G. Wallace, *Nat. Nanotechnol.* **2008**, *3*, 101.
[31] W. Li, C. Gao, *Langmuir* **2007**, *23*, 4575.
[32] D. A. Dikin, S. Stankovich, E. J. Zimney, R. D. Piner, G. H. B. Dommett, G. Evmenenko, S. T. Nguyen, R. S. Ruoff, *Nature* **2007**, *448*, 457.
[33] D. K. Nagesha, M. A. Whitehead, J. L. Coffer, *Adv. Mater.* **2005**, *17*, 921.
[34] T. Kokubo, H. Takadama, *Biomaterials* **2006**, *27*, 2907.
[35] Q. Shi, J. Wang, J. Zhang, J. Fan, G. D. Stucky, *Adv. Mater.* **2006**, *18*, 1038.
[36] G. He, T. Dahl, A. Veis, A. George, *Nat. Mater.* **2003**, *2*, 552.
[37] A. Antonakos, E. Liarokapis, T. Leventouri, *Biomaterials* **2007**, *28*, 3043.
[38] S. Kim, C. B. Park, *Biomaterials* **2010**, *31*, 6628.
[39] T. P. Kunzler, T. Drobek, M. Schuler, N. D. Spencer, *Biomaterials* **2007**, *28*, 2175.
[40] N. Ribeiro, S. R. Sousa, F. J. Monteiro, *J. Colloid Interface Sci.* **2010**, *351*, 398.
[41] M. A. Wozniak, K. Modzelewska, L. Kwong, P. J. Keely, *Biochim. Biophys. Acta* **2004**, *1692*, 103.
[42] E. Cukierman, R. Pankov, D. R. Stevens, K. M. Yamada, *Science* **2001**, *294*, 1708.
[43] J. Hu, X. Liu, P. X. Ma, *Biomaterials* **2008**, *29*, 3815.